Noise in Relaxation Oscillators

ASAD A. ABIDI AND ROBERT G. MEYER, FELLOW, IEEE

Abstract—**The timing jitter in relaxation oscillators is analyzed. This jitter is described by a single normalized equation whose solution allows prediction of noise in practical oscillators. The theory is confirmed by measurements on practical oscillators and is used to develop a prototype low noise oscillator with a measured jitter of 1.5 ppm rms.**

I. INTRODUCTION

LOW noise in the output of an oscillator is important in many applications. The noise produced in the active and passive components of the oscillator circuit adds random perturbations to the amplitude and phase of the oscillatory waveform at its output. These perturbations then set a limit on the sensitivity of such systems as receivers, detectors, and data transmission links whose performance relies on the precise periodicity of an oscillation.

A number of papers [1]–[6] were published over the past several decades in which theories were developed for the prediction of noise in high-Q LC and crystal oscillators which are widely used in high-frequency receivers. Noise in these circuits is filtered into a narrow bandwidth by the high-Q frequency-selective elements. This fact allows a relatively simple analysis of the noise in the oscillation, the results of which show that the signal to noise ratio of the oscillation varies inversely with Q.

Relaxation oscillators are an important class of oscillators used in applications such as voltage-controllable frequency and waveform generation. In contrast to LC oscillators, they require only one energy storage element, and rely on the nonlinear characteristics of the circuit rather than on a frequency-selective element to define an oscillatory waveform. These circuits have recently become common because they are easy to fabricate as monolithic integrated circuits.

Due to their broad-band nature, these oscillators often suffer from large random fluctuations in the period of their output waveforms, termed the *timing jitter*, or simply, *jitter* in the oscillator. In an application such as an FM demodulator, the relaxation oscillator in a phase-locked loop will be limited in its dynamic range, and hence sensitivity, due to this jitter. There are no systematic studies in the literature, however, on either measurements of jitter in relaxation oscillators, or on an analysis of how noise voltages and currents in the components of the oscillator randomly modulate the periodic waveform. Such an analysis was perhaps discouraged by the nonlinear fashion in which the oscillator operates, as shall become evident in Section III below.

Despite this state of affairs, circuits designers have successfully used methods based on qualitative reasoning to reduce the jitter in relaxation oscillators. The purpose of this study has been to develop an explicit background for these methods. By analyzing the switching of such oscillators in the presence of noise, circuit methods are developed to reduce the timing jitter.

The results of this study have been verified experimentally, and a prototype low jitter oscillator was built with jitter less than 2 parts per million, nearly an order of magnitude better than most commonly available circuits.

II. OSCILLATOR TOPOLOGIES AND DEFINITION OF JITTER

One of the most popular relaxation oscillator circuits is the emitter-coupled multivibrator [7] with a floating timing capacitor shown in Fig. 1, which uses bipolar transistors as the active devices. Transistors $Q1$ and $Q2$ alternately switch on and off, and the timing capacitor C is charged and discharged via current sources I. Transistors $Q3$ and $Q4$ are level shifting emitter followers, and diodes $D1$ and $D2$ define the voltage swings at the collectors of $Q1$ and $Q2$. A triangle wave is obtained across the capacitor and square waves at the collectors of $Q1$ and $Q2$.

This circuit is sometimes modified for greater stability against temperature drifts, and other types of active devices are used, but in essence it is always equivalent to Fig. 1. The oscillator operates by sensing the capacitor voltage and reversing the current through it when this voltage exceeds a predetermined threshold.

Another common relaxation oscillator is shown in Fig. 2(a), which uses a grounded timing capacitor. The charging current is reversed by the Schmitt trigger output, whose two input thresholds determine the peak-to-peak amplitude of the triangle wave across the capacitor. The block diagram of this circuit is shown in Fig. 2(b). As the ground in an oscillator is defined only with respect to a load, the circuit of Fig. 1 is also represented by the block diagram of Fig. 2(b).

Manuscript received November 16, 1982; revised April 14, 1983. This research work was supported by the U.S. Army Research Office under Grant DAAG29-80-K-0067.

A. A. Abidi is with the Bell Laboratories, Murray Hill, NJ 07974.

R. G. Meyer is with the Electronics Research Laboratory, University of California, Berkeley, CA 94720.

0018-9200/83/1200-0794$01.00

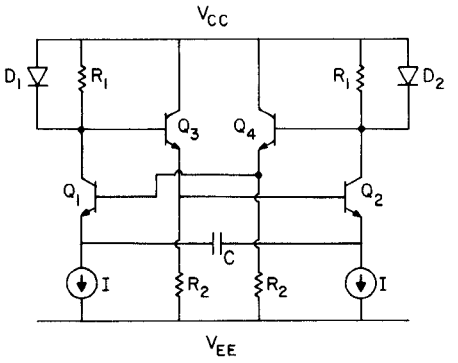

Fig. 1. Cross-coupled relaxation oscillator with floating timing capacitor.

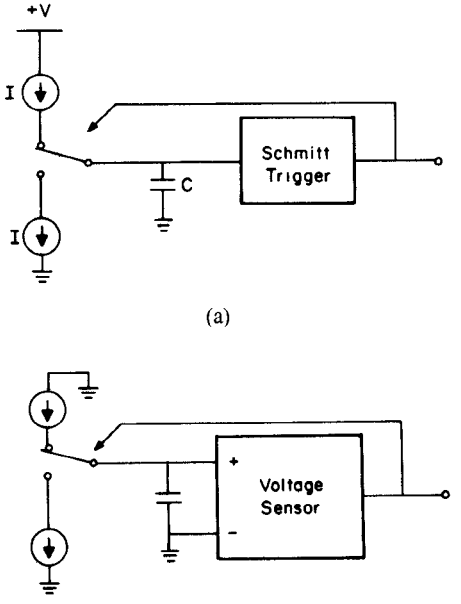

Fig. 2. (a) Relaxation oscillator with grounded timing capacitor. (b) Topological equivalent of oscillator.

The voltage sensor in such oscillators is a bistable circuit. When the capacitor voltage crosses one of the two trigger points at its input, the sensor changes state. The sensor has a vanishingly small gain, while the capacitor voltage is between these trigger points; but as a trigger point is approached, the operating points of the active devices in the sensor change in such a way that it becomes an amplifier of varying gain. The small-signal gain of the circuit is determined by an internal positive feedback loop, and becomes unboundedly large at the trigger point, causing the sensor to switch regeneratively and change the direction of the capacitor current.

In contrast to the linear voltage waveform on the capacitor (Fig. 3), the currents in the active devices of the sensor circuit are quite nonlinear because of this regeneration. The slope of these currents increases as the trigger point is approached, as shown in (Fig. 4), so that noise in the circuit is amplified and randomly modulates the time at which the circuit switches. Thus, the noisy current of Fig. 5 produces the randomly pulsewidth modulated waveform of

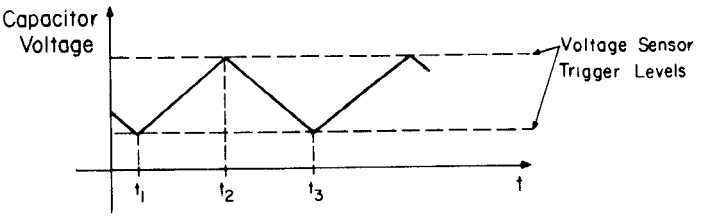

Fig. 4. Typical waveform of the current in a switching device in a relaxation oscillator.

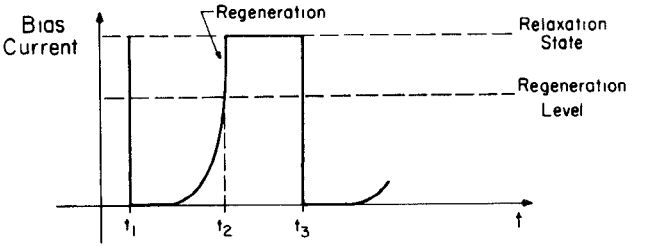

Fig. 4 Typical waveform of the current in a switching device in a relaxation oscillator.

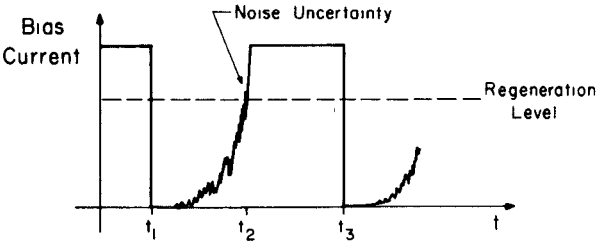

Fig 5 Actual waveform (including noise) of the current in a switching device in a relaxation oscillator.

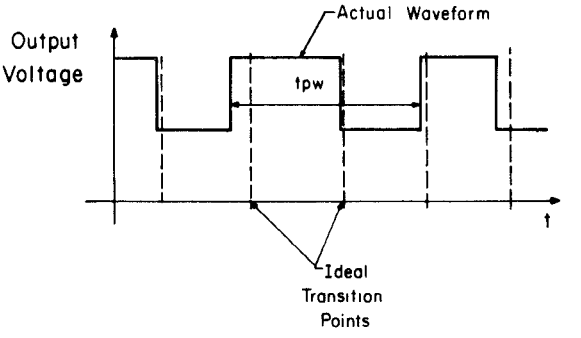

Fig. 6. Output voltage waveform of a relaxation oscillator showing the effect of noise.

Fig. 6. The timing jitter may be defined in terms of the mean μ_t and standard deviation σ_t of the pulsewidth as

$$\text{jitter} = \sigma_t/\mu_t \tag{1}$$

which is usually expressed in parts per million.

To determine the noise in FM demodulation, it is more desirable to know the frequency spectrum of an oscillation with jitter. However, the problem is more clearly stated, and solved, in the time domain, and the spectrum of the jitter should, in principle, be obtainable from a Fourier transformation.

III. The Process of Jitter Production

The switching of a floating capacitor oscillator in the presence of noise is now analyzed by examining the circuit of Fig. 7 as it approaches regeneration. The device and parasitic capacitance are assumed to be negligibly small. Suppose $Q2$ conducts a small current I_1, while $Q1$ carries the larger current $2I_0 - I_1$. The current flowing through the timing capacitor produces a negative-going ramp at V_4, causing an increase in $V_{BE}(Q_2)$ and thus in the current through Q_2. A single stationary noise source I_n is assumed to be present in the circuit, as shown in Fig. 7. The equations describing the circuit are

$$V_{BE_1} = V_T \log_e \frac{2I_0 - I_1}{I_S} \tag{2}$$

$$V_{BE_2} = V_T \log_e \frac{I_1}{I_S} \tag{3}$$

$$V_C = (2I_0 - I_1)R + V_{BE_2} - (I_1 - I_n)R - V_{BE_1} \tag{4}$$

$$\frac{dV_C}{dt} = \frac{I_0 - I_1}{C} \tag{5}$$

where $V_T = kT/q$ and I_S is the reverse leakage current at the base of the transistor.

Substituting (2) and (3) into (4), and applying (5), the differential equation describing the circuit is

$$\left(\frac{V_T}{2I_0 - I_1} + \frac{V_T}{I_1} - 2R\right)\frac{dI_1}{dt} + \frac{R\,dI_n}{dt} = \frac{I_0 - I_1}{C}. \tag{6}$$

This may be rewritten as

$$\frac{dI_1}{dt} = \left(\frac{1}{\dfrac{V_T}{2I_0 - I_1} + \dfrac{V_T}{I_1} - 2R}\right)\left(\frac{I_0 - I_1}{C} - \frac{R\,dI_n}{dt}\right) \tag{7}$$

where the right-hand side consists of two terms, one due to the autonomous dynamics of the circuit and one due to noise. As I_1 increases, the denominator of the right-hand side diminishes until it becomes zero when

$$I_1 = I_R \approx \frac{V_T}{2R} \tag{8}$$

where $I_1 \ll I_0$; I_1 must satisfy this inequality for the circuit to oscillate. I_R is defined as the *regeneration threshold* of the circuit: upon exceeding it, and in the absence of any device or stray capacitance, I_1 would change at an infinite rate until one of the circuit voltages limits. Accordingly, the circuit is said to be in the *relaxation mode* while $0 < I_1 < I_R$, and in *regeneration* when $I_R < I_1 < 2I_0$. (I_1 may be the current through either $Q1$ or $Q2$, depending on the particular half cycle of oscillation.)

Suppose that at some time $t = t_4$ the circuit is in relaxation so that the current $I_1 = I_A$, and that it builds up the threshold of regeneration $I_1 = I_R$ at time $t = t_2$. Equation

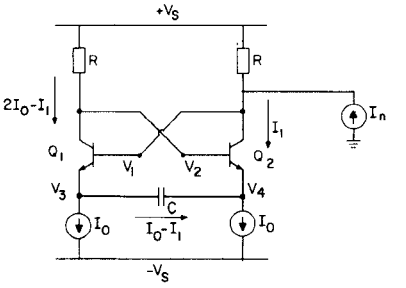

Fig. 7 Generalized equivalent circuit of a relaxation oscillator for noise analysis.

(6) can then be integrated from t_A to t_2 as follows:

$$\int_{I_A}^{I_R}\left(\frac{V_T}{2I_0 - I_1} + \frac{V_T}{I_1} - 2R\right)dI_1 = \int_{t_4}^{t_2}\left(\frac{I_0 - I_1}{C}\right)dt - R\{I_n(t_2) - I_n(t_A)\} \tag{9}$$

so that

$$V_K = \frac{I_0}{C}(t_2 - t_A) - \int_{t_A}^{t_2}\frac{I_1}{C}dt - R\{I_n(t_2) - I_n(t_A)\} \tag{10}$$

where V_K, the left-hand side of (9), is a constant which depends only on the choice of initial current I_A, I_0, and, from (8), on V_T and R.

The influence of the noise current on the instant of switching is now evident from (10): random fluctuations in the value of $I_n(t_2)$ must induce corresponding fluctuations in t_2 so that the sum of the terms on the right-hand side of (10) remains equal to the constant V_K. More precisely, if $t_A = 0$ and $t_2 = T$ (the half-period of the oscillation), then

$$F(I_n(T), T) \overset{\text{def}}{=} \frac{I_0}{C}T - \int_0^T \frac{I_1(t)}{C}dt - R\{I_n(T) - I_n(0)\} = \text{constant} \tag{11}$$

and thus

$$\delta F = \left.\frac{\partial F}{\partial I_n}\right|_T \delta I_n(T) + \frac{\partial F(I_n, T)}{\partial T}\delta T = 0 \tag{12}$$

which implies

$$-R\delta I_n(T) + \left\{\frac{I_0}{C} - \frac{I_1(T)}{C}\right\}\delta T = 0 \tag{13}$$

so that

$$\delta T = \frac{R}{\left\{\dfrac{I_0 - I_1(T)}{C}\right\}}\delta I_n(T). \tag{14}$$

By definition, $I_1(T) = I_R$ so

$$\delta T = \frac{R}{\left\{\dfrac{I_0 - I_R}{C}\right\}}\delta I_n(T). \tag{15}$$

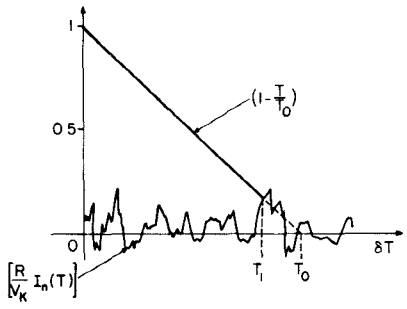

Fig. 8. Graphical interpretation of (19).

The main result of this paper lies in interpreting this equation as follows: the *variation* in switching times δT is equal to the variation in the times of first intersection of a *ramp* $(I_0 - I_R/C)T$ with the noise waveform $RI_n(T)$, as shown in Fig. 8. Note that the x axis in this figure is T, and *not* "real" time t. Thus, while the current waveform is nonlinear, as in Fig. 5, and while the time T, at which it starts to regenerate is given by the integral equation (10), *variations* in T appear as if they were produced by the first crossing of a noisy threshold by a linear ramp.

The statistics of T are contained in (10) in terms of the distribution of $I_n(t)$. This is the well-known equation for the first-crossings' distribution of a deterministic waveform with noise [8] and does not have a convenient closed form solution.

Nevertheless, a useful empirical result has been obtained for the distribution of T which allows the jitter in relaxation oscillators to be predicted quite accurately. This result is based on the following observations.

1) The linearized equation (15) describes completely the *deviations* in T; therefore, it contains information on the statistics of T.

2) It is plausible that the jitter will be directly proportional to the rms noise current for a fixed slope of the timing waveform.

3) If the dominant noise power in the oscillator lies at high frequencies, it acts to reduce the mean period of oscillation. This is evident from Fig. 8, where the ramp will almost always cross a positive-going peak of the noise.

4) If low-frequency noise is dominant, the resulting jitter will be greater than it would be if the same noise power were concentrated at higher frequencies. Again, Fig. 8 shows this, because if noise varies slowly compared to the ramp rate, the first-crossing will occur both above and below the x axis.

These observations can be quantitatively summarized as

$$\sigma(\delta T) = \sigma(T) = \alpha \frac{RC}{I_0 - I_R} \sigma(I_n) \tag{16}$$

where σ denotes the standard deviation of its argument and α is a constant of proportionality which by 1) and 2) above depends on whether the noise power is contained at high or at low frequencies. Equation (15) changes to (16) in going from the variation in T in one switching event to the standard deviation of an ensemble of such events.

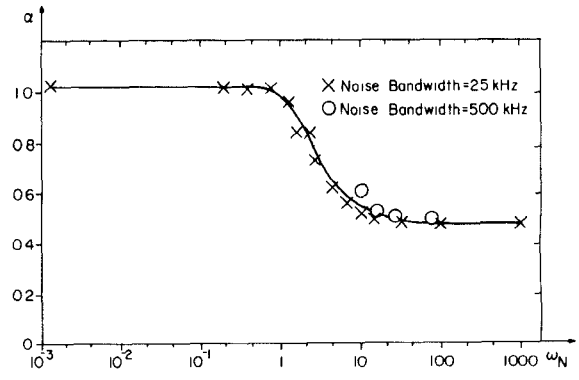

Fig. 9. Measured values of parameter α versus normalized noise bandwidth ω_N

The constant α varies with the relative slope of the ramp to the rms slope of the noise. For white noise which has been low-pass filtered, the rms slope can be defined relative to the ramp rate by ω_N, where

$$\omega_N \overset{\text{def}}{=} 2\pi \times \frac{\text{rms noise voltage} \times \text{noise bandwidth}}{\text{voltage ramp rate}} \tag{17}$$

and where the rms noise voltage is responsible for modulating the first-crossing instant of the voltage ramp of Fig. 8.

The dependence of α on ω_N for low-pass filtered white noise is shown in Fig. 9. It was obtained from measurements on different oscillator circuits, and at varying noise levels, as described in Section V of this paper. This dependence should be the same for white noise in any relaxation oscillator. For $\omega_N \ll 1$, α approaches unity, as 4) above suggests, because the deviation in oscillator period faithfully follows the meanderings of the noise waveform. For $\omega_N \gg 1$, α is asymptotic to about 0.5 because only the positive peaks of noise determine the first-crossing, in accordance with 3).

If the effect of all the noise sources in an oscillator is represented by the single source I_n, then using the appropriate α, the jitter in its output can be predicted by (16). For example, in Fig. 7 devices $Q1$ and $Q2$, while forward-biased, act as voltage followers for the various noise voltage sources in the circuit, so that I_n is the rms sum of these noise voltages divided by the node resistance at the collector. This is true for all noise sources except the noise current flowing through the timing capacitor which is integrated into a voltage by the capacitor. As shown in Appendix I, its contribution to the jitter is usually negligible.

IV. Interpretation and Generalization of Results

We emphasize that the linear result of (16), which describes the variations in the nonlinear waveform of Fig. 5, is not merely an outcome of an incremental analysis of the problem, which would go as follows. As the loop approaches regeneration, the dc incremental gain increases and the small signal bandwidth due to the device and

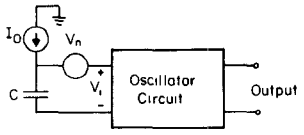

Fig. 10. Representation of noise in the relaxation oscillator by an equivalent input generator V_n.

parasitic capacitance decreases in inverse proportion, so that the incremental gain is infinite and the bandwidth zero at the onset of regeneration. Having entered the regeneration regime, the effect of the capacitance is to limit the maximum rate of change of the circuit waveforms. Thinking in terms of signal-to-noise ratio, the incremental device current is the signal which must compete with the amplified noise in the circuit to determine the time of switching. From the considerations of gain and bandwidth above, the rms value of white noise would become infinite at the regeneration threshold, so reducing the "signal"-to-noise ratio to zero. This implies infinite jitter, which is obviously not the case in reality. Such an approach demonstrates the inadequacy of thinking of this problem in terms of small signals.

A complete, large scale analysis shows that jitter production is better understood by thinking of the oscillator as the simplified threshold circuit of Fig. 10. The equivalent noise at the input of the circuit adds to the linear voltage waveform on the timing capacitor to produce an uncertainty in the time of regeneration. It is important to realize that Fig. 10 represents the oscillator only for an incrementally small time before the onset of regeneration.

This result is independent of the type of the oscillator circuit, and of the nature of the active devices used in it.

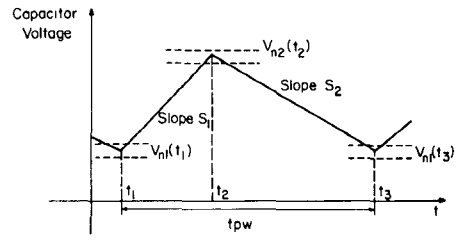

Fig. 11. Capacitor voltage waveform in a relaxation oscillator.

the measurement of the latter very difficult. By placing the oscillator in a phase-locked loop with a crystal-derived reference frequency, and by designing the loop filter with a cutoff well below the oscillation frequency, the thermal drift can be compensated, while the cycle-to-cycle jitter produced by noise frequencies above this cutoff remains unaffected. Appropriate precautions must be taken against fluctuations in the power supply, and against ground loop noise.

The effect of a noise voltage V_n over a complete cycle of oscillation is shown in Fig. 11, where the timing capacitor waveform is assumed to be asymmetrical for generality. As the device current I_1 in Fig. 7 always equals I_R at switching, the limits of the capacitor voltage have to fluctuate in response to the noise. Therefore, as the capacitor voltage is a continuous waveform, the fluctuations at times t_1, t_2, and t_3 all contribute to δT. Thus,

$$\delta T = \frac{V_n(t_1)}{S_1} + \frac{V_n(t_2)}{S_1} + \frac{V_n(t_2)}{S_2} + \frac{V_n(t_3)}{S_2}. \quad (19)$$

The standard deviation of the random variable δT is

$$\sigma(\delta T) = \alpha \times \left\{ \text{mean value of} \left\{ \frac{V_n^2(t_1)}{S_1^2} + V_n^2(t_2)\left(\frac{1}{S_1} + \frac{1}{S_2}\right)^2 + \frac{V_n^2(t_3)}{S_2^2} \right\} \right\}^{1/2} \quad (20)$$

The analysis of the grounded capacitor oscillator in Appendix II, and further generalizations given elsewhere [10] show that the jitter in any relaxation oscillator is given by the following expression:

$$\text{jitter} = \frac{\text{rms noise voltage in series with timing waveform}}{\text{slope of waveform at triggering point}} \times \text{a constant}. \quad (18)$$

V. Experimental Results

To verify the formulas for phase jitter developed above, and also to develop low noise oscillator circuits, it is necessary to be able to measure jitter with a resolution of about 1 ppm. This entails obtaining the distribution of pulsewidths from an accurate pulsewidth meter while the oscillator runs at a low frequency; the jitter is then the standard deviation of this distribution. However, the short-term thermal drift of the oscillation frequency can overwhelm the variations in cycle-to-cycle jitter, making

where $V_n(t_1)$, $V_n(t_2)$, and $V_n(t_3)$ are statistically independent values of the noise voltage $V_n(t)$, and α is the constant of proportionality defined in (16). When $S_1 = S_2 = S$ in magnitude,

$$\sigma(\delta T) = \alpha\sqrt{6}\,\frac{V_n(\text{rms})}{S} \quad (21)$$

where $\sigma(\delta T)$ is the jitter.

Measurements were made by dominating the oscillator's internal noise sources by an externally injected low-pass filtered white noise current. Two different oscillator circuits, described below, were used to obtain the experimental data. Histograms for the distributions of pulsewidths for injected noise with $\omega_N = 0.2$ and 1000 are shown in Fig. 12, where this range of ω_N was obtained by adjusting both the power and bandwidth of the injected noise. These histograms are unimodal and approximately symmetric, and they fit the normalized Gaussian function to within experimental error. Such experiments were also used to obtain the curve of α versus ω_N of Fig. 9, with the jitter defined as the standard deviation of these histograms.

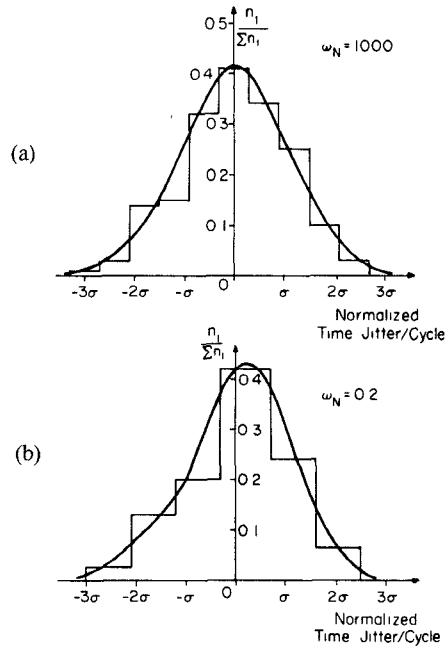

Fig. 12. Measured distributions of time jitter per cycle in the AD537 oscillator with (a) $\omega_N = 1000$ and (b) $\omega_N = 0.2$; fractional number of samples of single pulses versus their pulse widths.

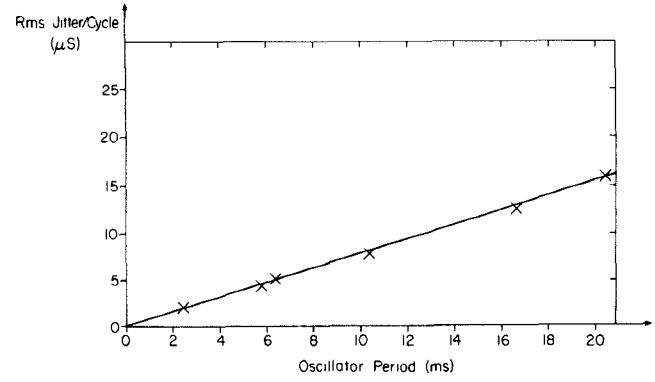

Fig. 13. Measured jitter per cycle versus oscillator period with noise injected into the AD537.

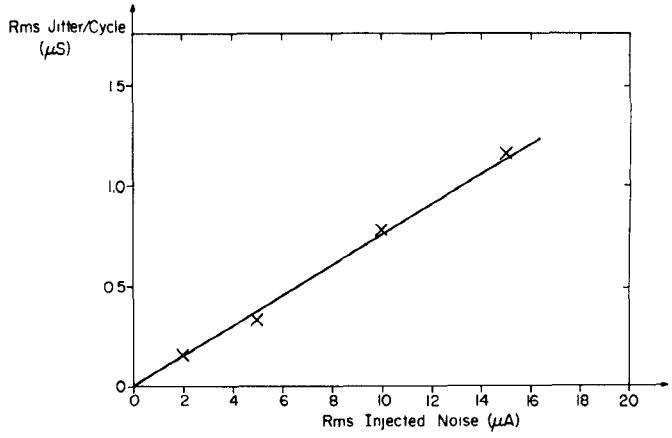

Fig. 14. Measured jitter per cycle versus injected noise amplitude in a grounded capacitor oscillator.

To verify the general result of (18), the following experiments were performed:

1) For a fixed injected rms noise, the jitter was measured as a function of the period of oscillation; the results are shown in Fig. 13.

2) For a fixed period of oscillation, the jitter was measured for a varying rms input noise; the results are plotted in Fig. 14.

The straight line fit of the data confirmed (18). In both 1) and 2), the range of the independent variable was restricted such that $\omega_N \gg 1$, thus ensuring that α was at its lower asymptotic value of 0.48, so that variations in α did not confound the measurements. The data of Fig. 13 were obtained from the AD 537 [9] floating capacitor oscillator, with a noise voltage applied in series with the voltage reference; Fig. 14 was obtained from measurements on a discrete component grounded capacitor oscillator [10], with a noise current injected into the Schmitt trigger. The reduction in mean period of oscillation predicted by 3) in Section III was also observed.

The most important application of this theory is in determining the jitter due to the inherent noise sources in an oscillator circuit. However, it is essential to know the bandwidth that applies to these noise sources in determining their total noise power. The small-signal bandwidth changes with the approach to the regeneration threshold when the circuit starts to behave like an integrator, as discussed in Section IV. While a detailed analysis of this is beyond the scope of this paper, the situation can be examined qualitatively. Consider the circuit described by (7) in the relaxation regime, and with all devices in the active region, when, say, $I_1 = 0.1 \times I_R$. If the spectrum of the superposition of all the noise sources on I_1 is considered as the "output" noise variable, the noise bandwidth of the circuit can be defined as the 3 dB down frequency of this spectrum. The equivalent input noise source of Fig. 10 is then this superposed noise in I_1 referred to a voltage source in series with the capacitor.

As I_1 approaches I_R, the circuit acts more like an integrator, so that fluctuations in the switching instant T are proportional to the fluctuations in the initial conditions of the integrator. The latter are simply produced by the noise in the circuit when the approach towards regeneration is started, which may roughly be defined as the time when $I_1 = 0.1 \times I_R$.

The spectral density of some of the noise sources in the circuit will depend on I_1, but usually they make a small contribution to the total noise, and their value at $0.1 \times I_R$ is a good approximation.

The noise bandwidth of the oscillator can be measured experimentally in two ways. The first relies on the availability of a white noise source with an adjustable output filter whose cutoff extends beyond the bandwidth to be measured. In response to a constant injected noise power, with the filter cutoff being progressively increased, the jitter will drop by 3 dB at the noise bandwidth of the oscillator. Alternatively, if the noise source has a fixed cutoff frequency, it can be used to modulate the amplitude of a carrier frequency, which is then injected into the oscillator. The random modulation will produce jitter, and

as the carrier frequency is increased, the jitter will reduce by 3 dB at the noise bandwidth. This relies on the fact that while the jitter is determined by the amplitude fluctuations (Fig. 8), the frequency components of the injected noise are concentrated around the carrier frequency, and increase with it.

As an example, the inherent jitter of the AD 537 VCO can be predicted. The noise bandwidth was measured to be 16 MHz using the second method described above. This 16 MHz value gives a fair agreement with SPICE noise simulations of the circuit biased at $I_1 = 0.1 \times I_R$, despite the fact that the exact values of the device capacitances were not available. The noise spectral density was simulated to be 1.3×10^{-8} V/$\sqrt{\text{Hz}}$ using SPICE, and was primarily due to the current sources and the base resistances of the level shift and switching transistors. Thus,

$$V_n = 1.3 \times 10^{-8} \times \sqrt{16 \times 10^6} = 52\ \mu\text{V rms}$$

At an oscillation frequency of 1 kHz, the slope of the timing capacitor ramp was 2.6×10^3 V/s, giving $\omega_N = 2.01$ and thus $\alpha = 0.8$ from Fig. 9. The predicted jitter is

$$\sigma(T) = \sqrt{6} \times 0.8 \times \frac{52 \times 10^{-6}}{2.6 \times 10^3}$$
$$= 39 \text{ ns}$$
$$= 39 \text{ ppm.}$$

The measured jitter from several samples had a mean value of 35 ppm, an excellent agreement in view of the approximate values of the active device noise models.

VI. A Low Jitter Oscillator Circuit

Many applications require even lower values of jitter than that of the AD 537 which is one of the lowest jitter monolithic VCO's widely available. The theory developed in this paper allows oscillators to be designed to a specified noise performance; as an example, a circuit with 1 ppm jitter was designed.

In the block diagram of Fig. 10, suppose that the timing voltage on the capacitor is a triangle wave with a peak-to-peak value V and period T. The slope of the ramp is

$$S = 2V/T \tag{22}$$

so the fractional jitter is

$$J = \frac{\alpha\sqrt{6}}{2} \frac{V_n}{V} \tag{23}$$

where V_n is the rms noise voltage. Thus, to obtain a small jitter, it is necessary to reduce V_n and increase V within the constraints of the circuit. V is limited by the power supply of the circuit, and V_n depends on both the characteristics of the active devices and the circuit topology. In the AD 537 topology (Fig. 15), for example, many devices additively contribute to the total noise in series with the timing capacitor because the functions of regeneration and threshold voltage detection are combined into one circuit.

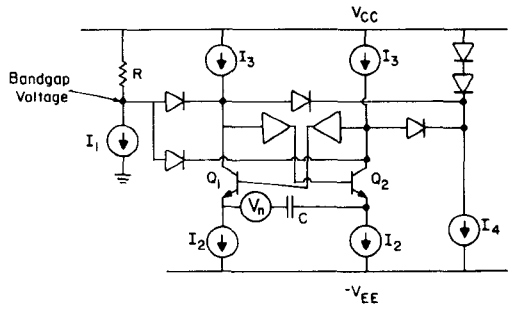

Fig. 15. Simplified schematic of the AD537.

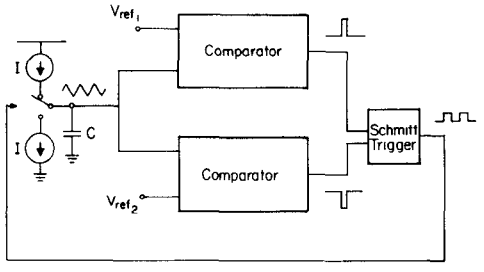

Fig. 16. Low-noise grounded capacitor oscillator topology.

In the grounded capacitor circuit [Fig. 2(a)], however, the current switch is separate from the regenerative Schmitt trigger; their noise contributions can thus be minimized independently.

Fig. 16 shows a variation of this topology where the Schmitt trigger is driven by fast pulses produced by high gain comparators following the timing capacitor. The result (18) shows that the contribution of the noise in the Schmitt trigger to the total jitter is inversely proportional to the slope of the waveform which drives it, and so is very small. Instead, the input noise of the comparators, which are driven by a slow ramp, determines the jitter. This scheme was used because very low input noise comparators are easily available, although there is no fundamental reason why a Schmitt trigger of comparable noise could not be designed. The complete schematic of the discrete component oscillator circuit is shown in Fig. 17. The differential comparators have a gain of 100 and an equivalent input noise of 6.3 μV rms over a noise bandwidth of 75 kHz. Using ± 6 V power supplies, the timing capacitor waveform was 8.8 V peak-to-peak, so (23) predicted the jitter to be 0.9 ppm rms. At an oscillation frequency of 1 kHz, the cycle-to-cycle jitter was measured to be 1.5 ppm rms; the additional jitter probably came from inadequate decoupling in the circuit.

An oscillator working from a single 5 V power supply with a jitter of about 1 ppm would be desirable in many systems applications. Such a circuit has been developed [12] on the basis of the results above, and the jitter measured to be less than 1 ppm at a 1 kHz oscillation frequency.

VII. Conclusions

Noise in relaxation oscillators can be described by a single normalized equation, which allows the jitter in any

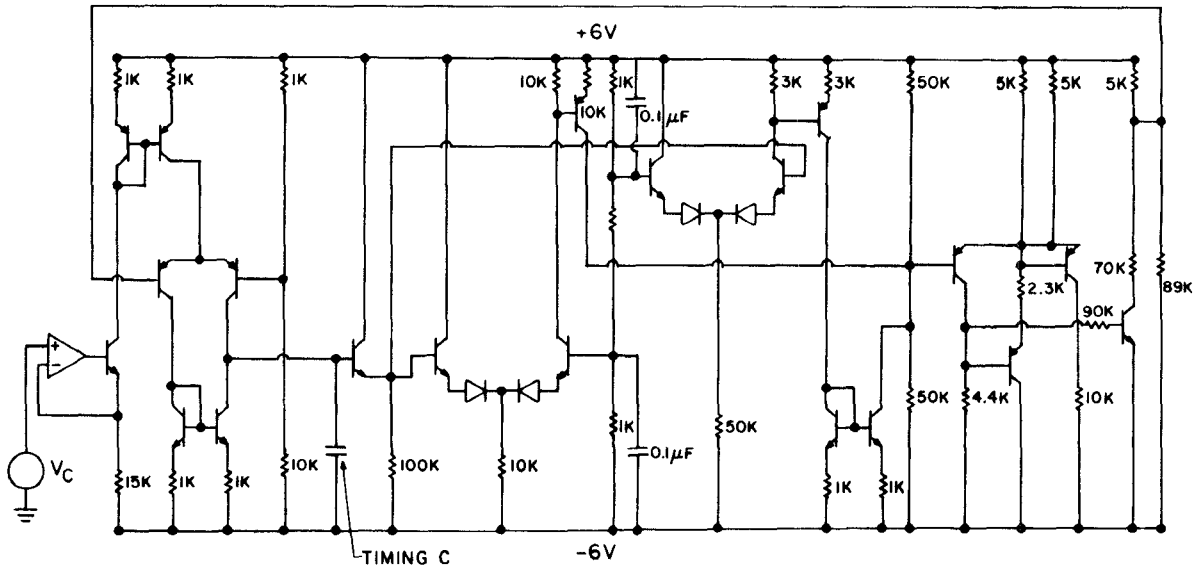

Fig. 17. Complete schematic for the low noise grounded-capacitor oscillator.

such oscillator to be predicted. The importance of this equation is that it linearizes the nonlinear regenerative waveforms in the oscillator. Further, it suggests those circuit topologies which promise low jitter, as demonstrated by an experimental prototype, whose jitter was measured to be 1.5 ppm at 1 kHz.

Appendix I

Effect of Noise Current Through the Timing Capacitor

In the schematics of Fig. 1 and Fig. 2 it can be seen that noise in the current sources appears directly in series the timing capacitor. In practice, these current sources are almost always active sources whose noise can be represented by a band-limited output noise current generator $I_{nc}(t)$. The capacitor then acts as a low-pass filter and the contribution V_{nc} from I_{nc} to the equivalent input noise voltage V_n of the oscillator (see Fig. 10) is

$$V_{nc}(t_r) = \frac{1}{C}\int_0^{t_r} I_{nc}(t)\,dt \qquad \text{(A1)}$$

where t_r is the time during which I_{nc} charges C. If I_{nc} is subject to a single-pole frequency roll off with bandwidth B and flat spectral density $S_{nc}(f)$, then it can be shown that [11]

$$(V_{nc})(\text{rms}) = \frac{1}{C}\sqrt{S_{nc}(f)} \times \sqrt{t_r} \qquad \text{(A2)}$$

where it is assumed that $t_r \gg 1/B$.

The rms noise contribution in V_n due to I_{nc} as given in (A2) can be compared with the contribution V_{nn} from I_n at the collector

$$(V_{nn})(\text{rms}) = (I_n)(\text{rms})R.$$

The relative importance of these two terms is now examined. Taking some typical values, if 1 mA current sources produce the shot noise,

$$S_{nc}(f) = 3.2\times10^{-22}\ \text{A}^2/\text{Hz}$$

and if $t_r = 1$ ms and $C = 0.5\ \mu$F, then from (A2)

$$(V_{nc})(\text{rms}) = 1.1\times10^{-6}\ \text{V}.$$

In comparison, when I_n is the shot noise in 1 mA of dc current, and it is band-limited to 16 MHz by the circuit capacitances, then $R = 500\ \Omega$ gives

$$(V_{nn})(\text{rms}) = \sqrt{3.2\times10^{-22}\times16\times10^{6}}\times500$$
$$= 36\times10^{-6}\ \text{V}.$$

Thus $V_{nc} \ll V_{nn}$, and the difference is even larger when additional contributions to V_{nn} are considered.

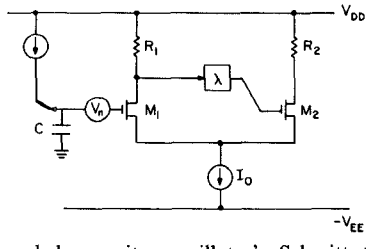

Fig. 18. Grounded capacitor oscillator's Schmitt trigger using MOS transistors.

Appendix II

Noise in an MOS Grounded Capacitor Oscillator

A simplified circuit of a grounded capacitor oscillator consisting of only the timing capacitor and the Schmitt trigger is shown in Fig. 18, where the latter uses MOS active devices with square law characteristics. The current I through device $M1$ is driven by the capacitor voltage and

makes the Schmitt trigger approach its regeneration threshold. The noise in the circuit is represented by the equivalent source V_n, and adds to the timing capacitor ramp in the manner of Fig. 10; it could equally well have been represented as a noise current source within the Schmitt circuit.

The circuit equations are as follows:

$$\frac{I_0 t}{C} + V_n = V_{GS_1} + V_S = V_T + \left(\frac{I}{\beta}\right)^{1/2} + V_S \tag{B1}$$

$$\lambda(V_{DD} - IR_1) = V_{GS_2} + V_S = V_T + \left(\frac{I_0 - I}{\beta}\right)^{1/2} + V_S. \tag{B2}$$

Subtracting (B2) from (B1)

$$\frac{I_0 t}{C} + V_n - \lambda V_{DD} + \lambda I R_1 = \left(\frac{I}{\beta}\right)^{1/2} - \left(\frac{I_0 - I}{\beta}\right)^{1/2} \tag{B3}$$

and differentiating (B3),

$$\frac{I_0}{C} + \frac{dV_n}{dT} + \lambda R_1 \frac{dI}{dt} = \frac{1}{2\beta}\left\{\left(\frac{\beta}{I}\right)^{1/2} + \left(\frac{\beta}{I_0 - I}\right)^{1/2}\right\}\frac{dI}{dt} \tag{B4}$$

rewriting which

$$\frac{dI}{dt} = \frac{\dfrac{I_0}{C} + \dfrac{dV_n}{dt}}{\dfrac{1}{2\beta}\left\{\left(\dfrac{\beta}{I}\right)^{1/2} + \left(\dfrac{\beta}{I_0 - I}\right)^{1/2}\right\} - \lambda R_1}. \tag{B5}$$

The regeneration threshold $I_R = 1/4\beta\lambda^2 R_1^2$ is the current at which the denominator of the right-hand side becomes zero. If this happens at $t = T$ relative to some time $t = 0$, then integrating (B5) from 0 to T gives

$$V_K = \frac{I_0 T}{C} + \{V_n(T) - V_n(0)\} \tag{B6}$$

where V_K is a constant voltage, depending only on the circuit parameters. This is exactly the same equation as (10), and gives the same result for jitter as (16).

References

[1] J. L. Stewart, "Frequency modulation noise in oscillators," *Proc. IRE*, vol. 44, pp. 372–376, Mar. 1956.

[2] W. A. Edson, "Noise in oscillators," *Proc. IRE*, vol. 48, pp. 1454–1466, Aug. 1960.

[3] J. A. Mullen, "Background noise in nonlinear oscillators," *Proc. IRE*, vol. 48, pp. 1467–1473, Aug. 1960.

[4] M. G. E. Golay, "Monochromaticity and noise in a regenerative electrical oscillator," *Proc. IRE*, vol. 48, pp. 1473–1477, Aug 1960.

[5] P. Grivet and A. Blaquiere, "Nonlinear effects of noise in electronic clocks," *Proc. IEEE*, vol. 51, pp. 1606–1614, Nov. 1963.

[6] J. Rutman, "Characterization of phase and frequency instabilities in precision frequency sources: Fifteen years of progress," *Proc. IEEE*, vol. 66, pp. 1048–1075, Sept. 1978.

[7] A. B. Grebene, "The monolithic phase-locked loop–A versatile building block," *IEEE Spectrum*, vol. 8, pp. 38–49, Mar. 1971.

[8] D. Middleton, *Statistical Communication Theory*. New York: McGraw-Hill, 1960.

[9] B. Gilbert, "A versatile monolithic voltage-to-frequency converter," *IEEE J. Solid-State Circuits*, vol. SC-11, pp. 852–864, Dec. 1976.

[10] A. A. Abidi, "Effects of random and periodic excitations on relaxation oscillators," Univ. California, Berkeley, Memo UCB/ERL M81/80, 1981.

[11] E. Parzen, *Stochastic Processes*. San Francisco: Holden-Day, 1962.

[12] T. P. Liu and R. G. Meyer, private communication.

Asad A. Abidi was born in 1956. He received the B.Sc. degree in electrical engineering with First Class Honors from Imperial College, London, England, in 1976, and the M.S. and Ph.D. degrees in electrical engineering from the University of California, Berkeley, in 1978 and 1981, respectively.

He has been a member of the Technical Staff at Bell laboratories, Murray Hill, NJ since 1981, where he is working on high-speed MOS analog integrated circuit design. His other main research interest is in nonlinear circuit phenomena.

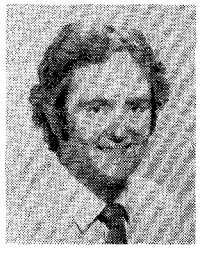

Robert G. Meyer (S'64–M'68–SM'74–F'81) was born in Melbourne, Australia, on July 21, 1942. He received the B.E., M.Eng.Sci., and Ph.D. degrees in electrical engineering from the University of Melbourne, Melbourne, Australia, in 1963, 1965, and 1968, respectively.

In 1968 he was employed as an Assistant Lecturer in Electrical Engineering at the University of Melbourne. Since September 1968, he has been with the Department of Electrical Engineering and Computer Sciences, University of California, Berkeley, where he is now a Professor. His current research interests are in integrated circuit design and device fabrication. He has been a Consultant to Hewlett-Packard, IBM, Exar, and Signetics. He is coauthor of the book *Analysis and Design of Analog Integrated Circuits* (Wiley, 1977), and Editor of the book *Integrated Circuit Operational Amplifiers* (IEEE Press, 1978). He is also President of the IEEE Solid-State Circuits Council and is a former Associate Editor of the IEEE JOURNAL OF SOLID-STATE CIRCUITS and of the IEEE TRANSACTIONS ON CIRCUITS AND SYSTEMS.